Heliyon 10 (2024) e36234

Contents lists available at ScienceDirect

Heliyon

journal homepage: www.cell.com/heliyon

Research article

Comprehensive analysis and experimental verification of the mechanism of anoikis related genes in pancreatic cancer

Qian Bao [a,b,1], Dongqian Li [a,b,1], Xinyu Yang [c,1], Shiqi Ren [b], Haoxiang Ding [b], Chengfeng Guo [b], Jian Wan [a], Yicheng Xiong [a], MingYan Zhu [a,**], Yao Wang [a,*]

[a] Department of Hepatobiliary and Pancreatic Surgery, Affiliated Hospital of Nantong University, Medical School of Nantong University, Nantong, Jiangsu, 226001, China
[b] Nantong University Medical School, Nantong, Jiangsu, 226001, China
[c] Research Center of Clinical Medicine, Affiliated Hospital of Nantong University, Medical School of Nantong University, Nantong, China

ARTICLE INFO

Keywords:
Pancreatic cancer
Anoikis
Gene signature in clinical prognosis
Single-cell analysis

ABSTRACT

Background: Pancreatic cancer (PC), characterized by its aggressive nature and low patient survival rate, remains a challenging malignancy. Anoikis, a process inhibiting the spread of metastatic cancer cells, is closely linked to cancer progression and metastasis through anoikis-related genes. Nonetheless, the precise mechanism of action of these genes in PC remains unclear.
Methods: Study data were acquired from the Cancer Genome Atlas (TCGA) database, with validation data accessed at the Gene Expression Omnibus (GEO) database. Differential expression analysis and univariate Cox analysis were performed to determine prognostically relevant differentially expressed genes (DEGs) associated with anoikis. Unsupervised cluster analysis was then employed to categorize cancer samples. Subsequently, a least absolute shrinkage and selection operator (LASSO) Cox regression analysis was conducted on the identified DEGs to establish a clinical prognostic gene signature. Using risk scores derived from this signature, patients with cancer were stratified into high-risk and low-risk groups, with further assessment conducted via survival analysis, immune infiltration analysis, and mutation analysis. External validation data were employed to confirm the findings, and Western blot and immunohistochemistry were utilized to validate risk genes for the clinical prognostic gene signature.
Results: A total of 20 prognostic-related DEGs associated with anoikis were obtained. The TCGA dataset revealed two distinct subgroups: cluster 1 and cluster 2. Utilizing the 20 DEGs, a clinical prognostic gene signature comprising two risk genes (CDKN3 and LAMA3) was constructed. Patients with pancreatic adenocarcinoma (PAAD) were classified into high-risk and low-risk groups per their risk scores, with the latter exhibiting a superior survival rate. Statistically significant variation was noted across immune infiltration and mutation levels between the two groups. Validation cohort results were consistent with the initial findings. Additionally, experimental verification confirmed the high expression of CDKN3 and LAMA3 in tumor samples.
Conclusion: Our study addresses the gap in understanding the involvement of genes linked to anoikis in PAAD. The clinical prognostic gene signature developed herein accurately stratifies patients with PAAD, contributing to the advancement of precision medicine for these patients.

* Corresponding author.
** Corresponding author.
E-mail addresses: 13809085661@163.com (M. Zhu), wanyao12274@163.com (Y. Wang).
[1] The authors contributed equally to this work: Qian Bao, Dongqian Li and Xinyu Yang.

https://doi.org/10.1016/j.heliyon.2024.e36234
Received 13 April 2024; Received in revised form 30 July 2024; Accepted 12 August 2024
Available online 13 August 2024
2405-8440/© 2024 The Authors. Published by Elsevier Ltd. This is an open access article under the CC BY-NC-ND license (http://creativecommons.org/licenses/by-nc-nd/4.0/).

1. Introduction

Pancreatic cancer (PC) manifests as an invasive tumor with aggressive malignant potential, and its 5-year survival rate is notably low. The global incidence rate and mortality associated with PC are increasing significantly, with current trends indicating its rise to the second position as a contributor to cancer-linked deaths by 2030 [1,2]. As a malignancy within digestive tract cancers, PC exhibits characteristics such as rapid progression and a high mortality rate [3,4]. Potential risk factors for PC include the consumption of alcohol, a high-fat and protein diet, smoking, high coffee intake, genetic elements, and environmental pollution. Pancreatic ductal adenocarcinoma (PDAC) constitutes ~90 % of PC cases and is one of its common pathological types. Due to the unclear early symptoms of pancreatic adenocarcinoma (PAAD), many patients often experience delayed diagnosis, resulting in a significant number of late-stage diagnoses accompanied by distant metastasis. This situation leads to missing the optimal treatment window for radical surgery [5–7]. Currently, an integrated approach involving surgery, adjuvant therapy, neoadjuvant therapy, and immunotherapy is commonly utilized for PAAD patients but only exhibits effectiveness in 20 % of patients [8–11]. Challenges such as postoperative recurrence, widespread tolerance to radiotherapy and chemotherapy, insensitivity to immunotherapy, and sustained low treatment response persist in the management of PAAD. Consequently, this contributes to poor treatment efficacy and a bleak prognosis for patients with PAAD, with its 5-year survival rate of merely 10 % [12–15]. The etiology and pathogenesis of PAAD remain incompletely understood, underscoring the pressing need to identify biomarkers and therapeutic targets for PAAD. Such advancements are necessary to enhance the quality of life and overall survival (OS) of the afflicted patients.

Anoikis, a programmed cell death mechanism, serves as a crucial defense for microorganisms and is induced by the loss of the interaction between cells and the extracellular matrix (ECM) [16,17]. Under normal circumstances, the disruption of the interaction between cells and the ECM, caused by the loss of adhesion promoters and glycosylated ECM proteins on the cell surface, leads to normal cell apoptosis and death. However, tumor cells are shielded by a protective "barrier" that is responsible for preventing the loss of adhesion promoters, generating cell death resistance, and promoting tumor cell survival [18,19]. Among various human tumors, anoikis acts as a protective physiological barrier, inhibiting the spread of metastatic cancer cells. Consequently, inhibiting anoikis becomes a critical mechanism for the development of cancer metastasis [20–22]. Recent research suggests a strong association of anoikis-related genes with cancer progression and metastasis. For instance, FAIM2 is significantly linked to tumor staging and adverse outcomes in non-small cell lung cancer, and reduced FAIM2 expression may hinder resistance to loss-of-nest (adhesion) apoptosis [23]. A study by Wang et al. demonstrated that CPT1A-mediated fatty acid oxidation can inhibit anoikis, promoting the metastasis of colorectal cancer cells [24]. Prior research has investigated the involvement of anoikis-related genes in diverse human malignancies like renal clear cell carcinoma, lung cancer, bladder cancer, hepatocellular carcinoma, etc. [25–28] However, there is a limited body of research systematically exploring the involvement of anoikis-related genes in PAAD.

Therefore, the primary aim of this research is to develop a prognostic scoring model utilizing anoikis-related genes. Additionally, it seeks to explore the relationship between this prognostic scoring model, the immune microenvironment, and chemotherapy sensitivity under the generated risk score. The objective is to analyze the clinical significance of this prognostic model in assessing the prognosis of patients with PAAD and characterize the immune landscape. Ultimately, these efforts seek to enhance the personalized treatment approach for patients with PAAD.

2. Methods

2.1. Data acquisition and processing

The genetic information of PAAD patients and their clinical details were accessed at TCGA and GEO. The TCGA-PAAD dataset comprised 179 tumor and 4 normal samples, while the GEO dataset (GSE78229) included 50 PAAD samples. Somatic mutation and copy number variation (CNV) data of patients with PAAD were accessed at the TCGA database. GeneCard database was searched to acquire the anoikis-related genes. To create a unified PAAD dataset, the TCGA-PAAD and GEO datasets were merged. To address batch processing effects across different datasets, the ComBat function from the R "SVA" package was employed. Subsequently, the "caret" package was utilized for random division of the PAAD dataset into a training group and a validation group.

2.2. Unsupervised cluster analysis based on anoikis-related genes

The expression of genes linked to anoikis was retrieved from the TCGA-PAAD dataset. Differential expression analysis was conducted for the identification of differentially expressed genes (DEGs) linked to anoikis. Subsequently, the identified DEGs were utilized for conducting unsupervised clustering analysis employing R "ConsensusClusterPlus". Additionally, DEGs between various subtypes were assessed via the "limma" R package."

2.3. Genomic variation analysis (GSVA) and functional enrichment analysis

Following the download of "c2. Cp. Kegg. V6.2. symbols" from the MsigDB database, GSVA enrichment analysis was executed using the R "GSVA" to investigate the biological pathways among different anoikis subtypes [29]. Utilizing the "limma" package, $P < 0.05$ was deemed as indicative of statistical significance between various subgroups. Subsequently, the "clusterProfiler" R package was employed to characterize potential biological processes, cellular components, molecular functions, and KEGG pathways of DEGs

between different subgroups. Significantly enriched biological pathways were determined per the threshold of $P < 0.05$.

Moreover, GSEA software was utilized to conduct GSEA analysis across high- and low-risk groups, aiming to identify the distinct KEGG pathways. Normalized enrichment scores (NES) and nominal P-values were calculated to assess the level of enrichment and statistical significance of the identified pathways.

2.4. Single sample gene set enrichment analysis algorithm (ssGSEA)

Utilizing ssGSEA, the correlation between the infiltration abundance of 23 immune cells and the subtypes associated with the loss-of-nest apoptosis was assessed through NES analysis.

2.5. Establishment and validation of gene signature for clinical prognosis utilizing DEGs

Univariate Cox analysis was employed to identify prognostically significant genes from DEGs between different subtypes, utilizing a threshold P-value lower than 0.05. The least absolute shrinkage and selection operator (LASSO) Cox regression model was then utilized to refine the pool of candidate genes and develop prognostic gene signatures. The formula for the clinical prognosis gene signature is as mentioned:

Risk score = (Expression of gene1 × β1) + (Expression of gene2 × β2) + (Expression of gene3 × β3) + … + (Expression of geneN × βN). Here, β denotes the regression coefficient.

As per the median risk score, patients in the training and validation groups underwent stratification into high-risk and low-risk groups. The variation in survival rates between the risk groups was examined via Kaplan-Meier curves. Heat maps were utilized to visually represent the expression of genes involved in constructing gene signatures in both groups. The model was assessed concerning its predictive performance through the area under the receiver operating characteristic (ROC) curve (AUC).

2.6. Development of predictive column charts

Furthermore, a column chart model was established using the risk score in conjunction with various clinical features. Furthermore, the survival rates of the patients with PAAD were predicted across 1, 3, and 5 years using the “rms” and “survival” packages. To examine the discrimination and accuracy of the column chart, calibration curves were employed.

2.7. Analysis of tumor microenvironment (TME) infiltration, somatic mutation, and immune checkpoint in various risk groups

CIBERSORT was utilized to examine the association of the risk score with the infiltration level of immune cells. The analysis of somatic cell variation data was conducted via R “maftools” [30]. To visually depict the mutation landscape in PAAD patients within the two risk groups, a waterfall plot was employed.

2.8. Exploring the drug sensitivity analysis of gene signature in clinical prognosis

Furthermore, leveraging the Cancer Drug Sensitivity Genomics (GDSC) database, drug response predictions were conducted using the “pRRophetic” R-package. Ridge regression was then applied for the estimation of the median maximum inhibitory concentration (IC50) for every patient, with the accuracy of the prediction analyzed through 10-fold cross-validation [31].

2.9. Analysis and identification of single cell RNA sequencing data

A single-cell dataset (GSE214295) was acquired from GEO, comprising three PAAD samples. To guarantee result quality, R “Seurat” was employed for preprocessing the data. This involved measuring the total number of molecules in cells (nCount RNA) and the genes identified in each cell (nFeature RNA). Furthermore, the gene number was comparatively assessed with the sequencing reads acquired from each cell. To assess widespread mitochondrial genome contamination in dead or low-quality cells, the percentage feature set function was employed to calculate the number of reads associated with the mitochondrial genome. Afterward, cell clustering was conducted utilizing filtered principal components, and unified manifold approximation and projection (UMAP) dimensionality reduction techniques were applied for visual classification. Marker genes for immune cells were filtered out with a corrected P-value <0.05. The marker genes acquired via the PanglaoDB database were intersected with the corresponding genes of each cell subtype to determine the specific immune cells. The resulting data provided insights into the correlation between the genes involved in constructing the gene signature and the single-cell subpopulation.

2.10. Western blotting assay

Phostphate-buffered saline (PBS) solution was used to rinse the cell culture flasks, followed by the addition of ice-cold lysis buffer (Servicebio, Wuhan, China). Cell lysates collected at 12,500 rpm and 4 °C were subjected to a 10-min boiling process in a super-sampling buffer. The proteins were then separated on a 12.5 % SDS-PAGE gel, along with a subsequent transfer to a PVDF membrane with a 0.2 μm

pore size. To minimize non-specific binding, 5 % skim milk was used for blocking.

The primary antibodies utilized were: CDKN3 (1:1000; ab175393, abcam, US), LAMA3 (1:1000; ab242197, abcam, US) and ACTIN (1:5000; Servicebio, Wuhan, China). Following the dilution of primary antibodies for CDKN3 and LAMA3 as per the provided protocol, overnight incubation was performed on a shaker at 4 °C. Subsequently, a 2 h incubation of the secondary antibody was carried out at 25 °C with slow shaking. The PVDF membrane underwent three washes with PBS, and immunoreactivity was visualized using the ECL Plus kit. To normalize the relative protein levels, calibration was performed based on the concentration of ACTIN.

2.11. Clinical specimens and immunohistochemistry (IHC)

A total of 13 cases of PAAD tumor tissues and their corresponding adjacent non-cancerous lung tissues were procured from the Affiliated Hospital of Nantong University (China). The study was subjected to approval by the Ethics Committee of Nantong University Hospital, with the provision of written informed consent deemed necessary for inclusion in the research and for the utilization of the

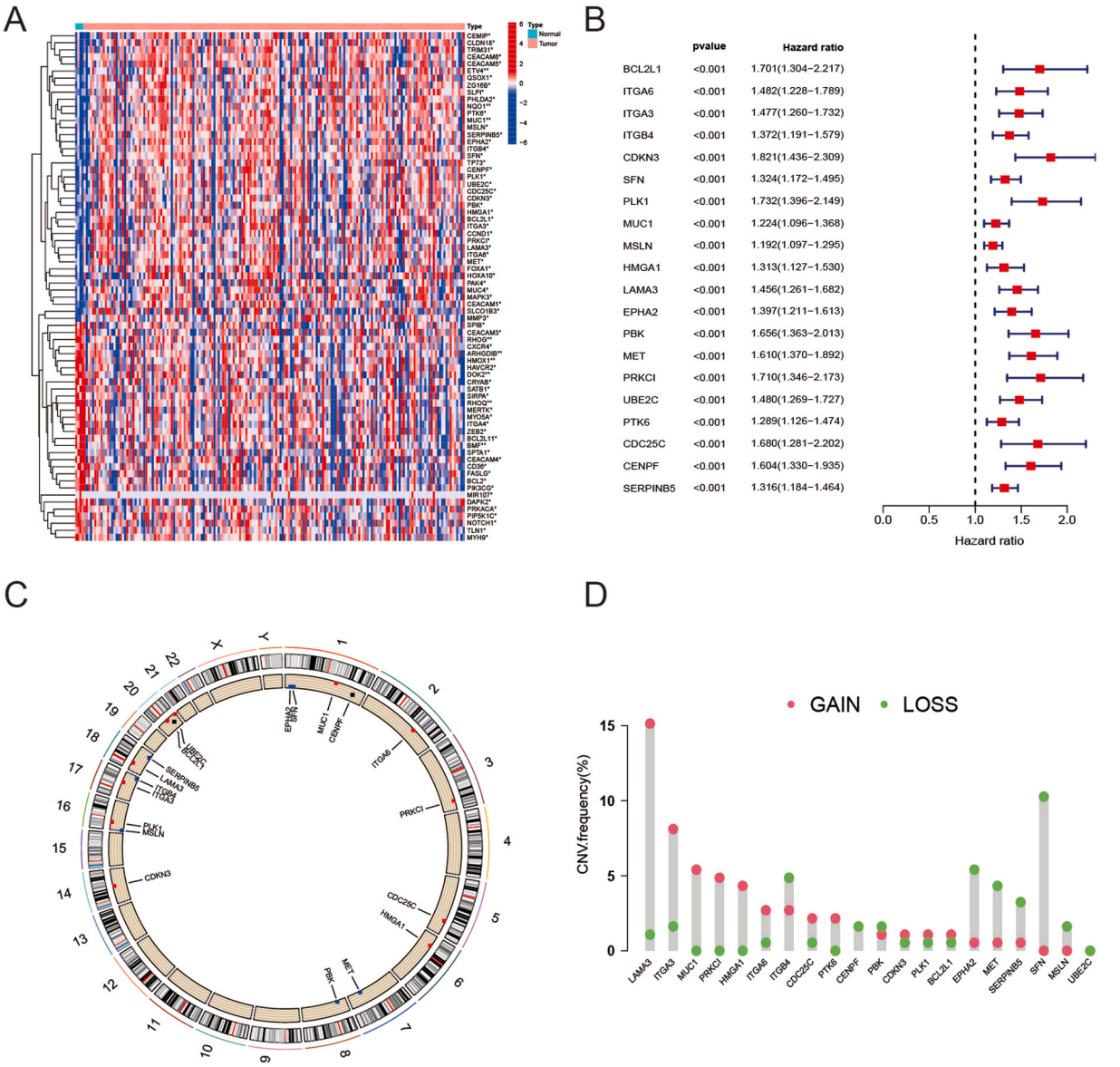

Fig. 1. Expression and genetic changes of anoikis-related genes in PAAD. (A) Heat maps displaying the differentially expressed genes (DEGs) between tumor samples and normal samples in the TCGA-PAAD cohort. (B) Identification of anoikis-related genes associated with prognosis in the PAAD cohort. (C) Chromosomal locations of CNV changes in anoikis-related regulatory factors. (D) Frequency of CNV variations in anoikis-related regulatory factors, with column height representing the change in frequency. Green dots indicate missing frequency, while the red dot indicates amplification frequency.

patient material.

The tissue sections underwent dewaxing, and antigens were extracted. After blocking with bovine serum albumin, sections were incubated with the PDXK primary antibody (1:200) at 4 °C overnight and rinsed thrice with PBS. Following 30 min incubation with the secondary antibody at 37 °C, DAP staining of the sections was performed for 5–10 min and hematoxylin for 10 s. Immunohistochemical staining was evaluated by assessing the intensity and extent of staining. The percentage of positive cells was scored as mentioned: ≤25 % (1 point), 26%–50 % (2 points), 51%–75 % (3 points), and >75 % (4 points). The intensity of the staining was categorized as follows: no positive staining (negative; 0 points), pale yellow (weakly positive; 1 point), tan (positive; 2 points), and sepia (strongly positive; 3 points). The two scores were multiplied to derive the final immunoreactivity score (IRS), assessing the level of protein staining. A score of 4 was utilized as the cutoff point to categorize the patients into high- and low-expression groups.

2.12. Statistical analysis

To conduct the statistical analyses, R v4.01 was utilized. The comparative assessment of two groups was conducted via the Wilcoxon test, while two or more groups were comparatively assessed via the Kruskal-Wallis test. Kaplan-Meier analysis and the logarithmic rank test were employed to assess survival differences among patients in different groups. Pearson correlation analysis was applied to evaluate the correlations. Principal component analysis (PCA) of different subtypes and risk groups was constructed through the "limma" package. To conduct the ROC curve analysis, R "survival" and "timeROC" were employed. A significance level of $P < 0.05$ indicated the statistical significance.

3. Result

3.1. Expression and genetic changes of anoikis-related genes in PAAD

In the TCGA-PAAD cohort, data concerning the expression of 490 genes related to anoikis was extracted. Further assessment of the 179 tumor samples and 4 normal samples resulted in the identification of 72 anoikis-related DEGs (Fig. 1A). In the PAAD cohort, which combined the TCGA-PAAD and GEO datasets, univariate Cox analysis based on the 72 anoikis-related DEGs was utilized to identify 20 relevant genes (Fig. 1B). These genes were then employed in subsequent analyses. Fig. 1C illustrates the positions of regulatory factors

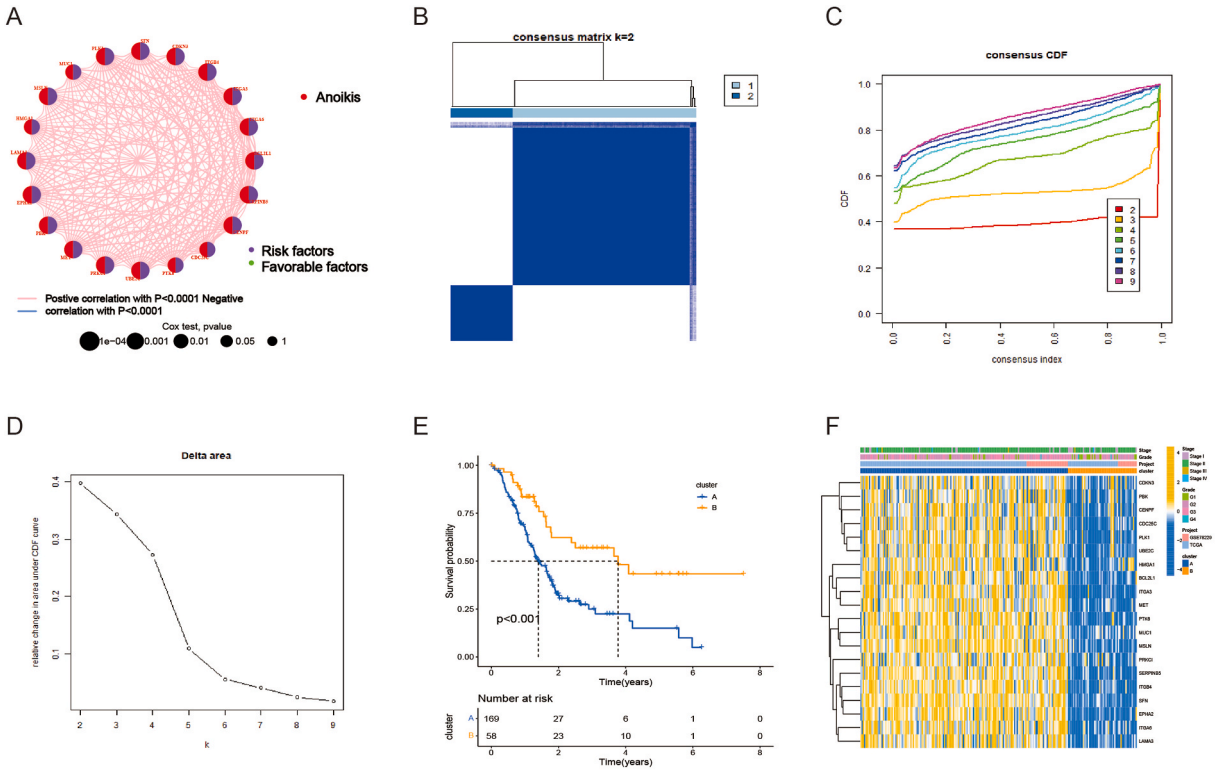

Fig. 2. Identification of anoikis-related subgroups in PAAD. (A) Interaction relationships among anoikis-related genes. (B–D) Application of the consistency clustering algorithm to partition PAAD samples into two distinct subgroups, namely cluster A and cluster B. (B) Consistency matrix; (C) Cumulative distribution function (CDF) diagram; (D) Change in the area under the CDF curve relative to K = 2–9. (E) Overall survival rates across the four subgroups. (F) Variations in the expression of anoikis-related genes between the two subgroups.

related to anoikis in CNV changes. Among the 20 regulatory factors, 9 genes (ITGB4, CENPF, PBK, EPHA2, MET, SERPINB5, SFN, MSLN, and UBE2C) exhibited copy number deletion, while the remaining genes showed copy number amplification (Fig. 1D).

3.2. Identification of anoikis-related subtypes in PAAD

A network was established to depict the interaction relationships among 20 genes related to anoikis (Fig. 2A). Subsequently, unsupervised cluster analysis was carried out using these 20 anoikis-related genes, resulting in the identification of two distinct subtypes: cluster A and cluster B (Fig. 2B–D). Survival analysis results indicate that patients in cluster B exhibit better OS compared to those in cluster A (Fig. 2E). The heatmap illustrates the correlation and clinical pathological characteristics between clusters A and B (Fig. 2F).

3.3. Association of different anoikis-related subtypes with immune cell infiltration, and the biological pathways related to the subtypes

This research further explored the relationship between subtypes linked to anoikis and the infiltration of immune cells in tumors. It

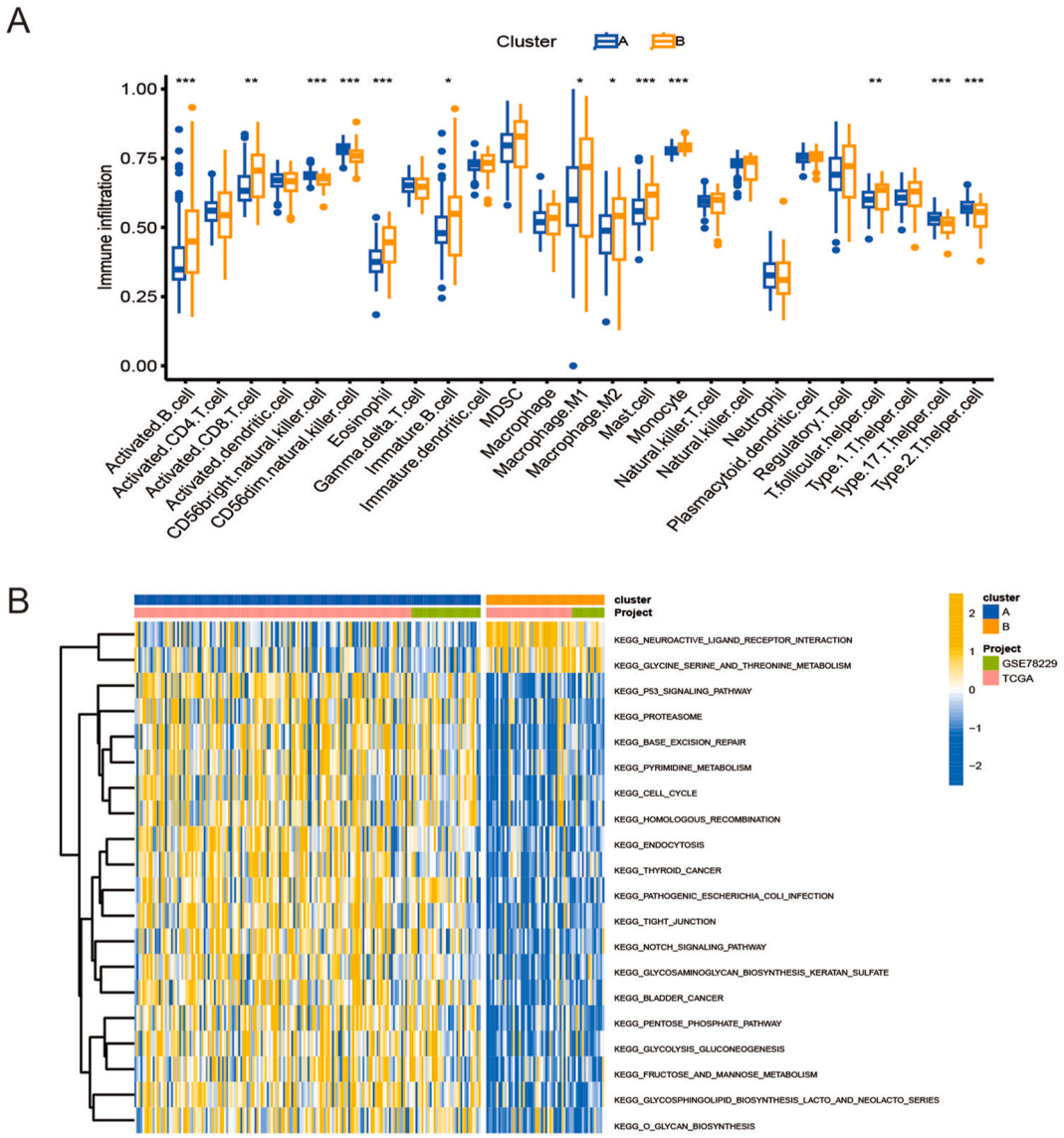

Fig. 3. Immune landscape characteristics and biological pathways between different subtypes in PAAD. (A) Variations in the abundance of immune infiltrating cells within the tumor microenvironment across different subgroups in PAAD. (B) GSVA enrichment analysis reveals the activation status of biological pathways between cluster A and cluster B. Heat maps illustrate these biological processes, where red and blue signify activated and inhibited pathways, respectively.

was noted that cluster B displays elevated levels of activated B cells, CD8T cells, eosinophils, immature B cells, mast cells, monocytes, and regulatory T cells. Conversely, cluster A exhibits an enrichment of CD56dim natural killer cells, CD56bright natural killer cells, type 2 T helper cells, and type 17 T helper cells (Fig. 3A).

Further investigation of the biological pathways linked to two diverse anoikis subtypes was carried out. Cluster A demonstrates a significant correlation with pathways, including the P53 pathway, cell cycle, and NOTCH pathway. On the other hand, cluster B is notably correlated with pathways such as glycine serine, neuroactive ligand-receptor interactions, and threonine metabolism (Fig. 3B).

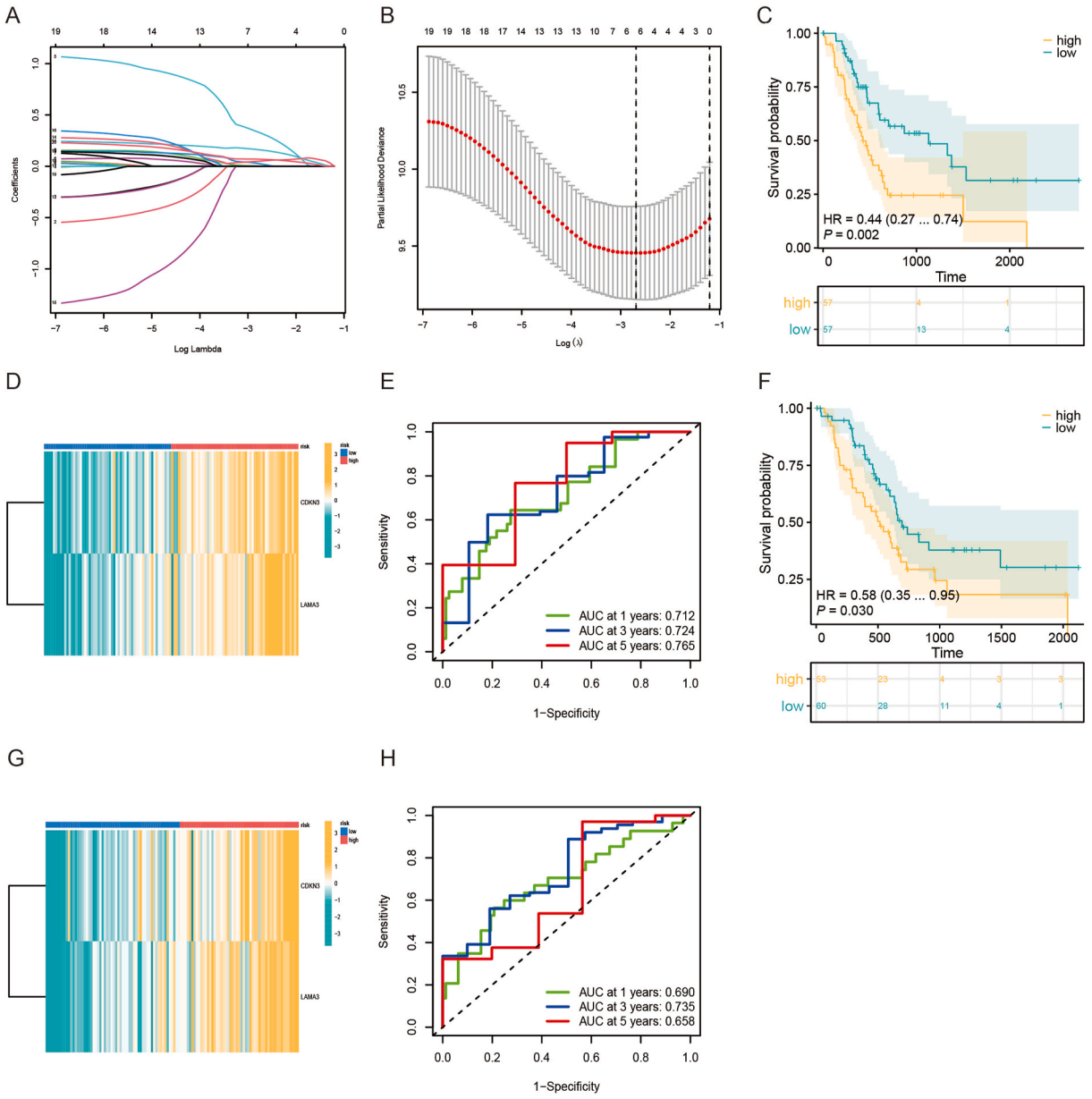

Fig. 4. Construction and validation of a clinical prognosis model. (A) Distribution of coefficients for prognostic genes in LASSO analysis. (B) A 10-fold cross-validation for optimizing the selection of parameters in LASSO analysis. (C) Comparison of overall survival time between patients with high- and low-risk PAAD. (D) Disparities in the expression of risk genes across the risk groups. (E) Survival rate prediction across 1, 3, and 5 years in the training group via ROC curve analysis. (F) Survival disparities between patients with high-risk and low-risk PAAD in the validation group. (G) Distribution of risk scores and survival status among different risk groups in the validation group, along with the expression of risk-associated genes in the two groups. (H) Survival rate prediction across 1, 3, and 5 years in the training group via ROC curve analysis.

3.4. Construction and validation of a gene signature for clinical prognosis based on anoikis-related genes

A gene signature for facilitating clinical prognosis was developed based on 20 genes associated with anoikis and prognosis. Utilizing LASSO-Cox regression analysis, two genes, CDKN3 and LAMA3, were identified as pertinent for constructing the signatures (Fig. 4A and B). The formula for the clinical prognosis gene signature is expressed as mentioned: risk score = (expression of CDKN3) * (0.5782) + (expression of LAMA3) * (0.3477).

In the training group, PAAD patients were classified, per the median risk value of the gene signature, into two risk groups (high and low). Kaplan-Meier analysis suggested that the low-risk patients displayed improved OS in comparison to those at higher risk (P = 0.001) (Fig. 4C). The heatmap illustrates the expression of the two risk genes utilized in constructing the gene signatures in patients from the two groups (Fig. 4D). Furthermore, the results of ROC analysis demonstrated that the gene signature effectively evaluates and predicts patient survival across 1, 3, and 5 years, with values of 0.712, 0.724, and 0.765, respectively (Fig. 4E).

Moreover, in the validation group, the efficacy of the gene signature in predicting clinical prognosis was examined. Stratification of patients with PAAD in the validation group into a high-risk and a low-risk group was executed per the median risk value of the gene signature. Kaplan-Meier analysis unveiled that patients in the low-risk group exhibited better OS relative to those in the high-risk group (P = 0.028) (Fig. 4F). The heatmap visually represents the expression of the two risk genes utilized in constructing the gene signatures in patients from the high-risk and low-risk groups (Fig. 4G).

Moreover, the results of ROC analysis confirm that the gene signature reliably evaluates and predicts patient survival across 1, 3, and 5 years in the validation group, with corresponding values of 0.696, 0.735, and 0.658, respectively (Fig. 4H).

3.5. Establishment of PAAD prognostic nomogram

Subsequently, a novel column chart was developed that integrates risk scores with other clinicopathological parameters to enhance the prediction of OS rates of patients across 1, 3, and 5 years. This results in optimizing the accuracy of the clinical prognosis of the gene signature (Fig. 5A). The calibration curves for the above-mentioned OS predictions of the column chart model we developed are illustrated in Fig. 5B. As time progresses, the accumulation of risk in patients categorized as low-risk is observed to be less than that in the patients at higher risk (Fig. 5C).

3.6. Association of the gene signature with immune cell and somatic mutations in clinical prognosis

Furthermore, the analysis explored whether any association existed between the gene signature and immune cells in terms of clinical prognosis. The study examined the relationship between the risk score and the degree of immune cell infiltration. The findings revealed a negative correlation between the risk score and the levels of B cells naive, Monocytes, and CD8 T cells, and a positive correlation with the levels of Dendritic cells activated. Interestingly, there was no significant correlation observed with the infiltration levels of immune cells like phagocytes (Supplementary Fig. 1).

The "maftools" package was employed to assess the risk groups concerning the disparity in the distribution of somatic mutations within the TCGA-PAAD cohort. As depicted in Fig. 6A and B, the high-risk group displayed a broader burden of tumor mutations in comparison to the low-risk group, with mutation frequencies of 77 % and 46 % for KRAS, respectively. High-risk patients were more correlated with high tumor mutational burden (TMB) values (P = 0.00083) (Fig. 6C). It was noted that patients with low TMB exhibited superior OS in comparison to those with high TMB (P = 0.008) (Fig. 6D). This trend persisted across both high- and low-risk populations, wherein the OS of patients with low TMB consistently outperformed that of patients with high TMB (P = 0.002) (Fig. 6E).

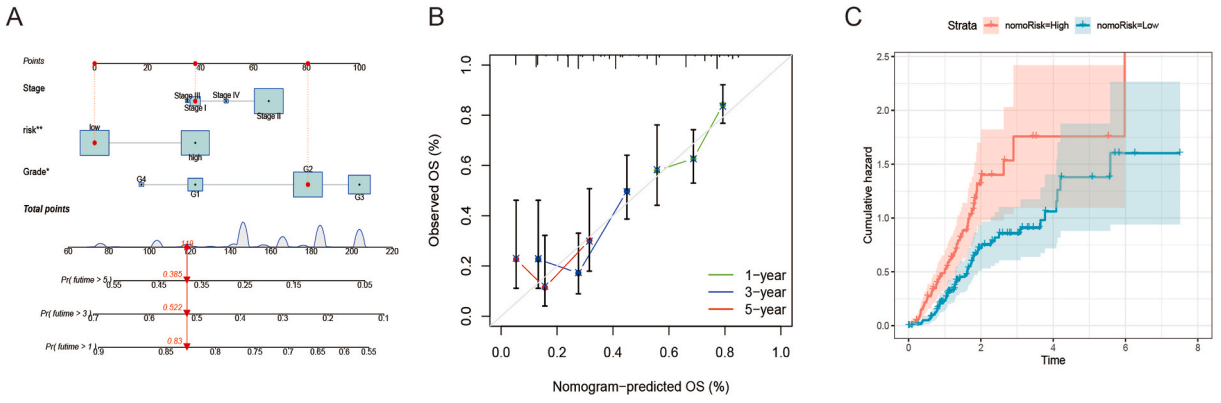

Fig. 5. Construction and evaluation of prognostic column charts in PAAD. (A) Column chart assessing 1-year, 3-year, and 5-year survival rates. (B) Calibration curve for the column chart. (C) Cumulative incidence rate based on risk stratification.

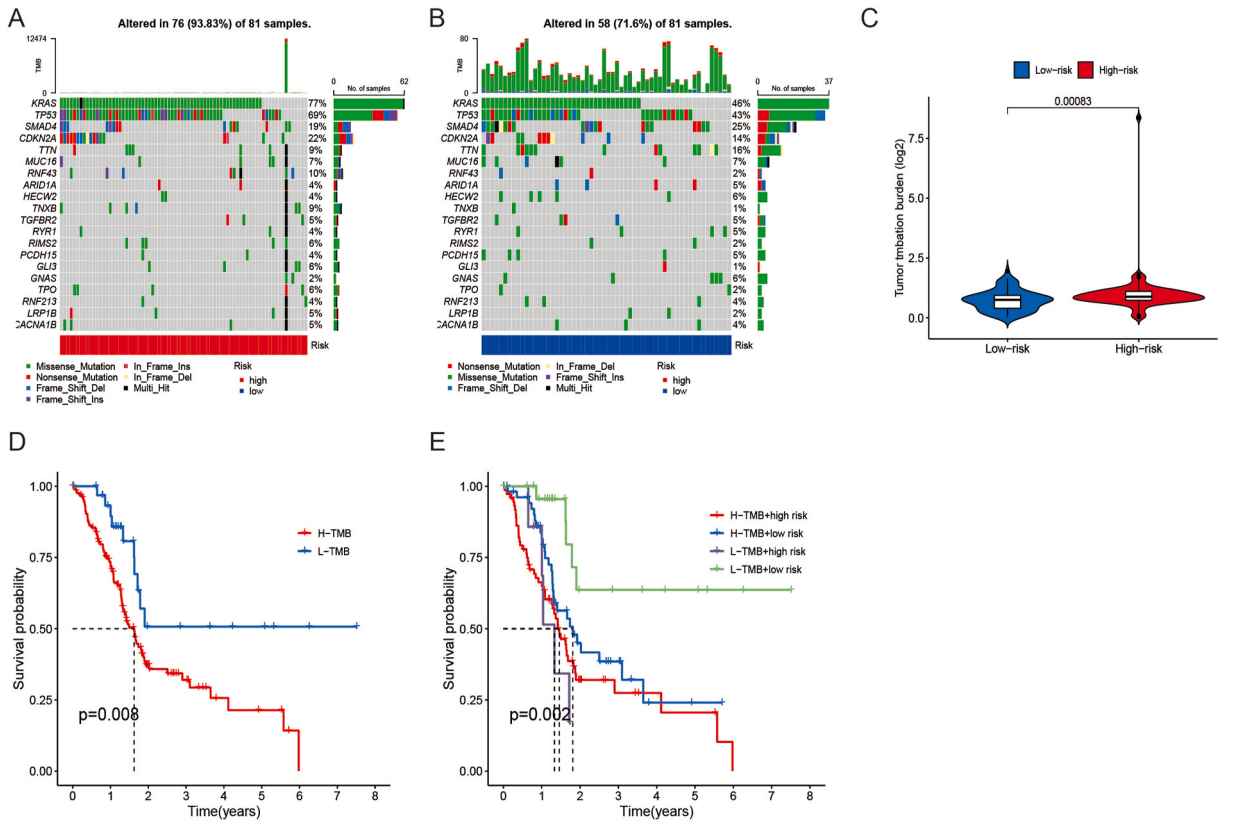

Fig. 6. Association between gene signature and somatic mutations in clinical prognosis. (A–B) Waterfall plot of tumor somatic mutations identified in patients from the risk groups. Each upper bar chart depicts TMB, with the number on the right indicating the mutation frequency of each gene. These columns represent individual patients. (A) High-risk group; (B) Low-risk group. (C) Association between risk score and TMB. (D) Variation in overall survival (OS) between patients with high and low TMB. (E) Within high and low-risk patient groups, OS in patients with low TMB consistently surpasses that of patients with high TMB.

3.7. Drug sensitivity analysis

The IC50 of each patient with PAAD was assessed using the pRRophetic algorithm. in comparison to the low-risk group, oxaliplatin in the high-risk group yielded a higher estimated IC50 value (Fig. 7A). Conversely, lapatinib, paclitaxel, and trametinib in the low-risk group displayed higher estimated IC50 values, indicating that high-risk patients are more likely to gain benefit from immunotherapy (Fig. 7B–D). We also investigated the relationship between checkpoint inhibitors and risk scores. Our findings suggest a positive correlation between the risk score and the expression of PDL1 and SIGLEC15 (Fig. 7E–H). This outcome suggests a higher likelihood of low-risk patients benefitting from immunotherapy.

3.8. Single-cell analysis

The GSE214295 data set containing three PAAD tissue samples was used for single-cell analysis. Fig. 8A and B illustrate the quality control and screening process for single-cell sequencing in PAAD samples. In PAAD tissue, a robust positive correlation exists between the measured gene expression and the gene count identified in cells. Conversely, gene expression observed in cells remains unaffected by the percentage of mitochondria. To maintain the quality of analyzed cells, cells with genes >2500 and <200 were filtered out, along with cells depicting mitochondrial percentages >5 %. PCA analysis of single-cell data is presented in Fig. 8C. A resolution of 1.5 was selected based on clustering tree results (Fig. 8D). The heatmap in Fig. 8E depicts the various types of each gene, while UMAP data reveal 33 cell clusters with diverse cell types labeled with distinct colors (Fig. 8F). CDKN3 is expressed in clusters 11, 23, and 32, while LAMA3 is expressed in clusters 0, 1, 2, 11, 16, 23, 27, 28, 31, and 33 (Fig. 8G). Utilizing the Cellmaker database, relevant genes were retrieved and intersected with genes associated with each UMAP cluster to annotate subgroups of different cell clusters (Fig. 8H). Fig. 8I demonstrates that the expression of CDKN3 and LAMA3 is associated with epithelial cells.

3.9. Validation of risk genes

Furthermore, thirteen PAAD tumor tissues and their corresponding adjacent non-cancerous lung tissues were analyzed for

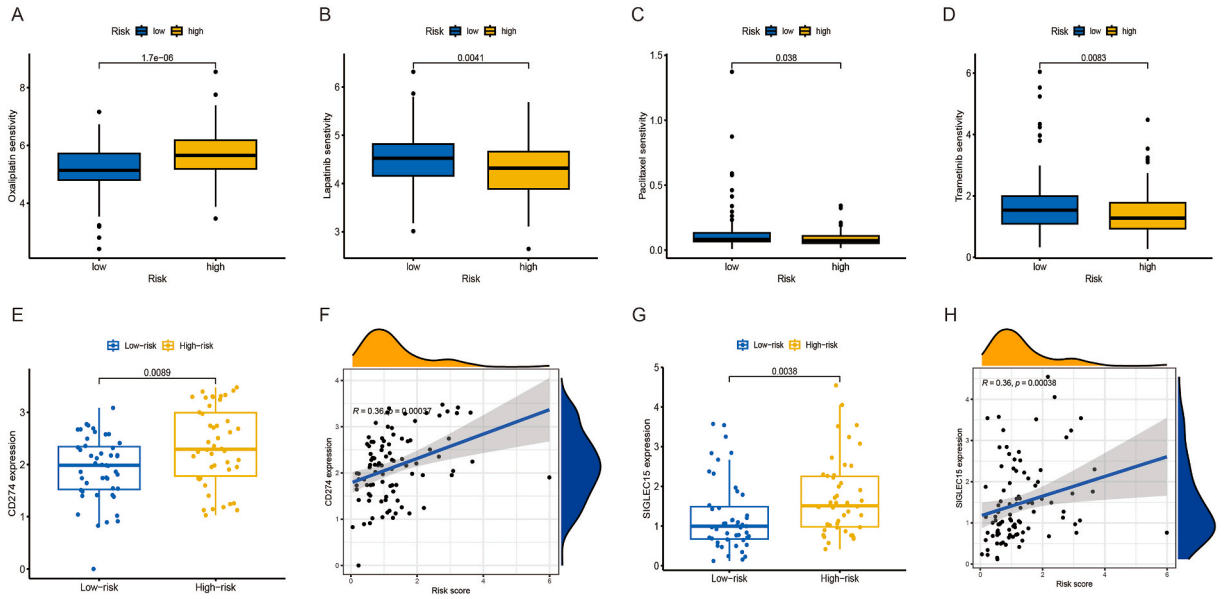

Fig. 7. Drug sensitivity analysis. Oxaliplatin, lapatinib, paclitaxel, and trametinib exhibit distinct IC50 values across the risk groups. (A) Oxaliplatin; (B) Lapatinib; (C) Paclitaxel; (D) Trametinib. (E) PDL1 is differentially expressed between high and low expression groups. (F) The risk score is positively correlated with the expression of PDL1. (G) SIGLEC15 is differentially expressed between high and low expression groups. (H) The risk score is positively correlated with the expression of SIGLEC15.

expression differences of CDKN3 and LAMA3 using IHC technology and Western blotting. IHC results demonstrated that the CDKN3 and LAMA3 levels were elevated in PAAD samples in comparison to paracancerous samples (Fig. 9A and B). Western blotting also revealed an elevated level of CDKN3 and LAMA3 proteins in PAAD samples (Fig. 9C and D).

4. Discussion

PAAD, characterized as an aggressive tumor, exhibits an extremely poor prognosis among patients. The high degree of heterogeneity in PAAD complicates efforts to improve patient outcomes, posing a significant challenge for researchers. The advancement of bioinformatics technology has facilitated disease research through the utilization of various public databases. This has resulted in advancing tumor research and propelling the exploration of novel therapeutic strategies. Previous evidence underscores the significance of constructing scoring models based on risk genes, aiding in the quantification of prognostic evaluation criteria and the development of personalized treatments [32–35].

In the present study, two PAAD-linked subtypes (cluster A and cluster B) were identified based on 20 prognostically relevant anoikis-related genes. Simultaneously, a PAAD-associated clinical prognostic gene signature was developed utilizing these 20 anoikis-related genes, featuring two risk genes (CDKN3 and LAMA3). This clinical prognostic gene signature demonstrated precision in stratifying patients with PAAD. Furthermore, the correlation between the clinical prognostic gene signature and immune cell and somatic cell mutations was assessed in-depth.

In this study, among the identified PAAD subtypes, cluster B displayed a remarkable survival advantage. Analysis of TME cell infiltration revealed a marked heterogeneity between these two subtypes. In the analysis of TME cell infiltration using the ssGSEA algorithm, an intriguing finding was observed. Both tumor-inhibiting $CD8^+$ T cells and tumor-promoting immunosuppressive cells exhibited high levels of infiltration within the same group simultaneously. This phenomenon is likely attributed to the intricate interactions occurring within the tumor microenvironment. $CD8^+$ T cells play a crucial role in immune responses by targeting and eliminating tumor cells. However, tumor cells often evade detection by the immune system through various mechanisms, such as recruiting immunosuppressive cells like regulatory T cells and tumor-associated macrophages (TAMs). TAMs are a subset of macrophages originating from monocytes, capable of producing immunosuppressive molecules within the tumor microenvironment to dampen immune cell activity, thereby facilitating tumor progression. The composition of immune cells in the tumor microenvironment undergoes dynamic changes influenced by factors such as tumor advancement, therapeutic interventions, and the host's immune status [36]. Additionally, GSVA analysis indicated that cluster A was notably associated with various pathways, including the P53 pathway, cell cycle, and NOTCH pathway. On the other hand, cluster B displayed remarkable associations with pathways like neuroactive ligand-receptor interactions, as well as glycine-serine and threonine metabolism.

The NOTCH signaling pathway, known to regulate various biological processes, including oncogenicity, was a key focus of this research [37–39]. Previous research has established that upon ligand binding, Notch receptor Notch intracellular structural domains (NICDs) are released, translocating to the nucleus. There, they bind to the transcriptional complex CSL/RBPJκ, activating the transcription of downstream target genes. This activation can further accelerate the progression of cancers, including PAAD [39–41].

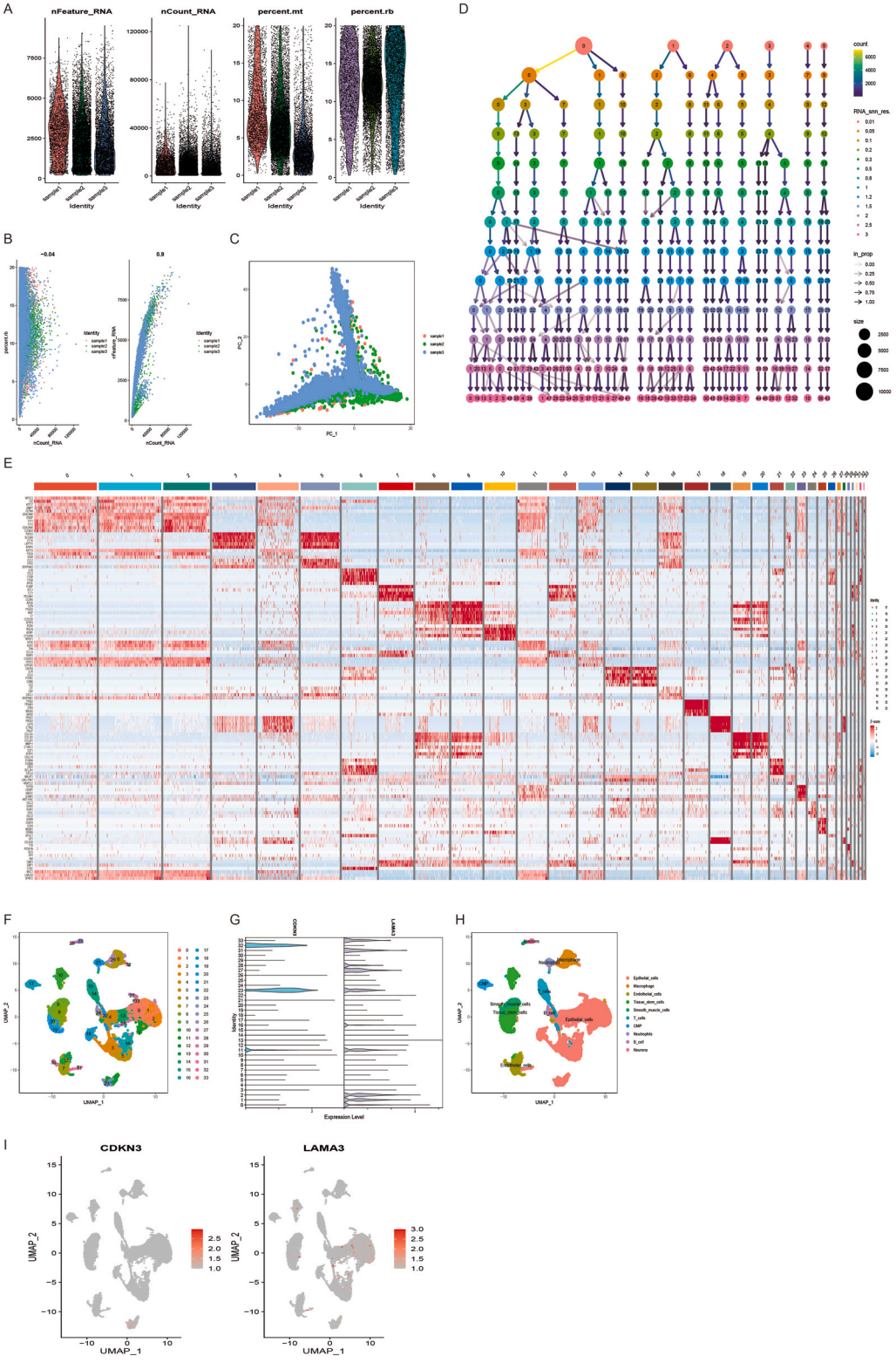

(caption on next page)

Fig. 8. Single-cell data analysis of characteristic genes for constructing gene signatures. (A) Quality control of single-cell data. (B) Correlation analysis between sequencing depth and mitochondrial genes. (C) Principal component analysis (PCA) of single-cell expression profile. (D) Selection of appropriate resolution based on the clustering tree. (E) Heat map displaying the marker genes for each subgroup. (F) UMAP algorithm illustrating 33 cell subpopulations. (G) Expression of characteristic genes for constructing gene signatures in various cell subpopulations. (H) Annotation of 33 cell subpopulations into 8 subpopulations. (I) Correlation between characteristic genes and cell subpopulations in constructing gene signatures.

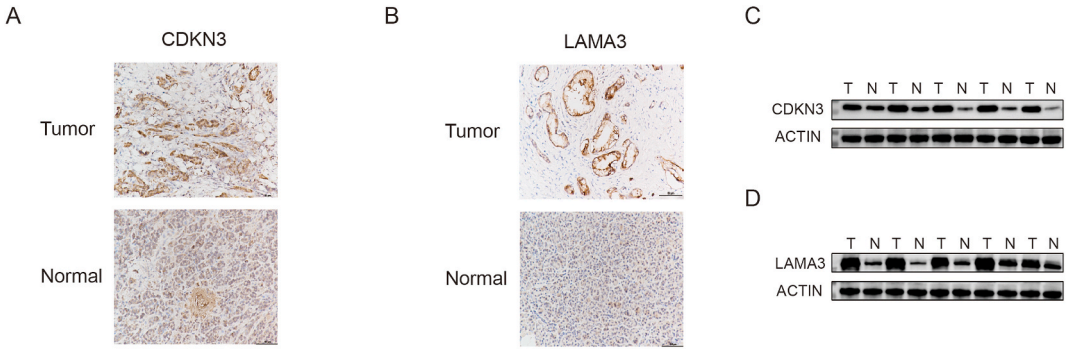

Fig. 9. Validation of risk genes for modeling. (A,B) IHC demonstrates the protein levels of CDKN3 (A) and LAMA3 (B) in tumor and normal samples. (B–D) Protein blot analysis depicting the expression of CDKN3 (C) and LAMA3 (D).

Notably, a study by Chen found that the Notch signaling pathway can be activated by RHBDL2, a highly active protein in PC tissues. The elevated level of RHBDL2 in PC tissues promotes the proliferative, migratory, and invasive capacities of PC cells both in vitro and in vivo, ultimately contributing to the development of PAAD [42]. Moreover, Wang et al. reported the existence of a positive association between Notch and IL-17. Their findings suggested that Notch activity can be upregulated by the IL-17 axis in vitro through the classic NF-κB pathway, synergistically promoting the development of PAAD [43]. Based on these observations, it is conjectured that the NOTCH signaling pathway may function as a crucial factor contributing to the poor prognosis of cluster A. Targeting the NOTCH signaling pathway could potentially aid in improving the survival status of patients within this cluster.

The clinical prognostic gene signature established herein effectively stratifies patients with PAAD, per their risk scores, into high- and low-risk groups, with the latter exhibiting a more favorable prognosis. The consistency in ROC results between the training and validation groups underscores the robust clinical predictive capability of the risk score. With the limited data available, we observed that patients in the low-risk group with pancreatic cancer had stable survival outcomes during a follow-up period of more than 7 years. This indicates the strong predictive capability of the model we developed and highlights significant differences in the prognosis of pancreatic cancer patients. While it is possible that the observed outcomes are influenced by the small sample size of our included studies, these findings do not undermine our conclusions. Furthermore, IHC validation confirmed the significant upregulation of the genes used to construct the model, namely CDKN3 and LAMA3, in PAAD tumor samples. CDKN3, belonging to the protein phosphatase family, has a pivotal function in cell cycle regulation [44,45]. Its involvement has been documented across various cancers, such as breast, prostate, ovarian, glioblastoma, hepatocellular, and renal cancers [46–49]. Ma et al. suggest that PSMD12, in collaboration with CDKN3, may influence cell cycle regulation through ubiquitination. Specifically, PSMD12 could modulate CDKN3 levels by interacting with it and reducing the ubiquitination level, thereby contributing to the development of PAAD [50]. LAMA3 encodes the α3 chain of laminin-5, a significant cell membrane component regulating cell adhesion and migration [51,52]. P Previous research indicates that LAMA3 accelerates tumor cell growth and invasion, positioning it as a promising target for cancer therapy [53]. A study by Yang reported a positive correlation between LAMA3 and blood flow in PDAC, suggesting LAMA3 as a possible therapeutic target and prognostic marker for this type of cancer [54]. While some studies have explored the mechanism of action of LAMA3 in various human tumors, there is a scarcity of research reports on its role in PAAD. Consequently, further investigations are warranted to unravel the molecular mechanisms that underlie LAMA3 in the context of PAAD.

In our current investigation, we observed a higher frequency of KRAS mutations in patients within the high-risk group relative to the low-risk group (77 %). Oncogenic KRAS mutations represent a pivotal event in the development of PC. The KRAS protein functions as a crucial signaling molecule, acting as a switch to regulate the activity of multiple intracellular signaling pathways. Mutations in the KRAS gene can lead to the sustained activation of the KRAS protein, preventing it from terminating signaling at the appropriate time. This sustained activation of KRAS continuously stimulates various intracellular signaling pathways and transcription factors, including MAPK, PI3K/AKT, and Raf. This, in turn, contributes to processes such as cell proliferation, migration, transformation, and survival. Through these mechanisms, KRAS mutations can foster uncontrolled proliferation and survival of PC cells, ultimately promoting the development and progression of PC [55–59]. We posit that this heightened frequency of KRAS mutations may be a contributing factor to the survival disadvantage observed in the high-risk group. Among anoikis-related genes, several have been identified to have connections to RAS. For instance, RAS mutations drive proliferative chronic myelomonocytic leukemia through PLK1 [60]. Moreover, heightened MET Translation and Signaling support K-Ras-driven proliferation in conditions of anchorage-independent growth [61]. Furthermore, EPHA2 has been linked to erlotinib resistance in K-RAS mutant pancreatic cancer [62]. As KRAS stands as the key

oncogene in over 80–90 % of PAAD cases, it represents a primary target for these oncogene-addicted tumors. However, the complex and diverse nature of KRAS mutations poses a significant challenge in identifying effective targeted therapeutic strategies for PC.

This investigation possesses certain limitations. First, our analysis relied solely on public data sourced from the TCGA database and the GEO database. Second, our experimental procedures were limited to IHC experiments conducted on genes modeled by PAAD; we did not conduct in vivo and in vitro experiments for validation. Consequently, there is a need to broaden the sample size and substantiate the robustness of PAAD-associated subtypes, as well as assess the clinical significance of the developed gene signature through additional prospective studies in the future.

5. Conclusion

The study unveiled two apoptosis-associated subtypes of PAAD, each demonstrating distinct clinical outcomes. The clinical gene signature developed in this investigation proves its efficacy in accurately predicting patient prognosis and guiding clinical medication for patients with PAAD. In summary, this investigation is important for further understanding the loss-of-nest apoptosis mechanism in PC and enhancing the current landscape of personalized treatment for patients with PAAD.

Ethics approval and consent to participate

The experimental protocol was developed in accordance with the ethical guidelines of the Declaration of Helsinki and approved by the Ethics Committee of Nantong University Hospital (2021-L068). Each subject provided written informed consent to participate in the experiment.

Consent for publication

The authors agrees to publication in the Journal.

Availability of data and material

The raw data supporting the conclusions of this manuscript will be made available by the corresponding authors, without undue reservation, to any qualified researcher.

Funding

Nantong Science and Technology Bureau (MS22022002).

CRediT authorship contribution statement

Qian Bao: Writing – original draft, Conceptualization. **Dongqian Li:** Writing – original draft, Conceptualization. **Xinyu Yang:** Writing – review & editing, Validation. **Shiqi Ren:** Writing – original draft, Conceptualization. **Haoxiang Ding:** Software, Data curation. **Chengfeng Guo:** Software, Data curation. **Jian Wan:** Validation, Formal analysis. **Yicheng Xiong:** Validation, Formal analysis. **MingYan Zhu:** Writing – review & editing, Conceptualization. **Yao Wang:** Writing – review & editing, Conceptualization.

Declaration of competing interest

The authors declare that they have no known competing financial interests or personal relationships that could have appeared to influence the work reported in this paper.

Acknowledgments

Not applicable.

Appendix A. Supplementary data

Supplementary data to this article can be found online at https://doi.org/10.1016/j.heliyon.2024.e36234.

References

[1] R.L. Siegel, K.D. Miller, H.E. Fuchs, A. Jemal, Cancer statistics, 2021, CA A Cancer J. Clin. 71 (1) (2021) 7–33.
[2] L. Rahib, B.D. Smith, R. Aizenberg, A.B. Rosenzweig, J.M. Fleshman, L.M. Matrisian, Projecting cancer incidence and deaths to 2030: the unexpected burden of thyroid, liver, and pancreas cancers in the United States, Cancer Res. 74 (11) (2014) 2913–2921.

[3] D. Ansari, B. Tingstedt, B. Andersson, et al., Pancreatic cancer: yesterday, today and tomorrow, Future Oncol. 12 (16) (2016) 1929–1946.
[4] C. Rizzato, D. Campa, R. Talar-Wojnarowska, et al., Association of genetic polymorphisms with survival of pancreatic ductal adenocarcinoma patients, Carcinogenesis 37 (10) (2016) 957–964.
[5] M.A. Tempero, NCCN guidelines updates: pancreatic cancer, J. Natl. Compr. Cancer Netw. : J. Natl. Compr. Cancer Netw. 17 (5.5) (2019) 603–605.
[6] S. Heinrich, H. Lang, Neoadjuvant therapy of pancreatic cancer: definitions and benefits, Int. J. Mol. Sci. 18 (8) (2017).
[7] Z. Zhao, W. Liu, Pancreatic cancer: a review of risk factors, diagnosis, and treatment, Technol. Cancer Res. Treat. 19 (2020), 1533033820962117.
[8] S. Wang, L. You, M. Dai, Y. Zhao, Mucins in pancreatic cancer: a well-established but promising family for diagnosis, prognosis and therapy, J. Cell Mol. Med. 24 (18) (2020) 10279–10289.
[9] J. Cai, H. Chen, M. Lu, et al., Advances in the epidemiology of pancreatic cancer: trends, risk factors, screening, and prognosis, Cancer letters 520 (2021) 1–11.
[10] F.G. Rocha, Landmark series: immunotherapy and targeted therapy for pancreatic cancer, Ann. Surg Oncol. 28 (3) (2021) 1400–1406.
[11] H.Y. Li, Z.M. Cui, J. Chen, X.Z. Guo, Y.Y. Li, Pancreatic cancer: diagnosis and treatments, Tumour biology : the journal of the International Society for Oncodevelopmental Biology and Medicine 36 (3) (2015) 1375–1384.
[12] Y.Z. Wang, Y. An, B.Q. Li, J. Lu, J.C. Guo, Research progress on circularRNAs in pancreatic cancer: emerging but promising, Cancer Biol. Ther. 20 (9) (2019) 1163–1171.
[13] J.J. Hue, K. Sugumar, S.C. Markt, et al., Facility volume-survival relationship in patients with early-stage pancreatic adenocarcinoma treated with neoadjuvant chemotherapy followed by pancreatoduodenectomy, Surgery 170 (1) (2021) 207–214.
[14] P. Weibel, M. Pavic, N. Lombriser, S. Gutknecht, M. Weber, Chemoradiotherapy after curative surgery for locally advanced pancreatic cancer: a 20-year single center experience, Surgical oncology 36 (2021) 36–41.
[15] J.H. Chang, Y. Jiang, V.G. Pillarisetty, Role of immune cells in pancreatic cancer from bench to clinical application: an updated review, Medicine 95 (49) (2016) e5541.
[16] F.O. Adeshakin, A.O. Adeshakin, L.O. Afolabi, D. Yan, G. Zhang, X. Wan, Mechanisms for modulating anoikis resistance in cancer and the relevance of metabolic reprogramming, Front. Oncol. 11 (2021) 626577.
[17] Y.N. Kim, K.H. Koo, J.Y. Sung, U.J. Yun, H. Kim, Anoikis resistance: an essential prerequisite for tumor metastasis, International journal of cell biology 2012 (2012) 306879.
[18] M. Raeisi, M. Zehtabi, K. Velaei, P. Fayyazpour, N. Aghaei, A. Mehdizadeh, Anoikis in cancer: the role of lipid signaling, Cell Biol. Int. 46 (11) (2022) 1717–1728.
[19] G.M. Slattum, J. Rosenblatt, Tumour cell invasion: an emerging role for basal epithelial cell extrusion, Nat. Rev. Cancer 14 (7) (2014) 495–501.
[20] A.P. Gilmore, Anoikis, Cell Death Differ. 12 (Suppl 2) (2005) 1473–1477.
[21] M.C. Guadamillas, A. Cerezo, M.A. Del Pozo, Overcoming anoikis–pathways to anchorage-independent growth in cancer, J. Cell Sci. 124 (Pt 19) (2011) 3189–3197.
[22] R. Jinka, R. Kapoor, P.G. Sistla, T.A. Raj, G. Pande, Alterations in cell-extracellular matrix interactions during progression of cancers, International journal of cell biology 2012 (2012) 219196.
[23] K. She, W. Yang, M. Li, W. Xiong, M. Zhou, FAIM2 promotes non-small cell lung cancer cell growth and bone metastasis by activating the wnt/β-catenin pathway, Front. Oncol. 11 (2021) 690142.
[24] Y.N. Wang, Z.L. Zeng, J. Lu, et al., CPT1A-mediated fatty acid oxidation promotes colorectal cancer cell metastasis by inhibiting anoikis, Oncogene 37 (46) (2018) 6025–6040.
[25] Y. Liu, Z. Shi, J. Zheng, et al., Establishment and validation of a novel anoikis-related prognostic signature of clear cell renal cell carcinoma, Front. Immunol. 14 (2023) 1171883.
[26] J. Wang, Z. Luo, L. Lin, et al., Anoikis-associated lung cancer metastasis: mechanisms and therapies, Cancers 14 (19) (2022).
[27] Y.Y. Zhang, X.W. Li, X.D. Li, et al., Comprehensive analysis of anoikis-related long non-coding RNA immune infiltration in patients with bladder cancer and immunotherapy, Front. Immunol. 13 (2022) 1055304.
[28] Y. Chen, W. Huang, J. Ouyang, J. Wang, Z. Xie, Identification of anoikis-related subgroups and prognosis model in liver hepatocellular carcinoma, Int. J. Mol. Sci. 24 (3) (2023).
[29] G. Yu, L.G. Wang, Y. Han, Q.Y. He, clusterProfiler: an R package for comparing biological themes among gene clusters, OMICS A J. Integr. Biol. 16 (5) (2012) 284–287.
[30] A. Mayakonda, D.C. Lin, Y. Assenov, C. Plass, H.P. Koeffler, Maftools: efficient and comprehensive analysis of somatic variants in cancer, Genome Res. 28 (11) (2018) 1747–1756.
[31] P. Geeleher, N. Cox, R.S. Huang, pRRophetic: an R package for prediction of clinical chemotherapeutic response from tumor gene expression levels, PLoS One 9 (9) (2014) e107468.
[32] T. Liu, L. Chen, G. Gao, et al., Development of a gene risk signature for patients of pancreatic cancer, Journal of healthcare engineering 2022 (2022) 4136825.
[33] M. Wu, X. Li, R. Liu, H. Yuan, W. Liu, Z. Liu, Development and validation of a metastasis-related gene signature for predicting the overall survival in patients with pancreatic ductal adenocarcinoma, J. Cancer 11 (21) (2020) 6299–6318.
[34] B. Yang, J. Xie, Z. Li, et al., Seven-gene signature on tumor microenvironment for predicting the prognosis of patients with pancreatic cancer, Gland Surg. 10 (4) (2021) 1397–1409.
[35] M. Wu, X. Li, T. Zhang, Z. Liu, Y. Zhao, Identification of a nine-gene signature and establishment of a prognostic nomogram predicting overall survival of pancreatic cancer, Front. Oncol. 9 (2019) 996.
[36] I. Kaymak, K.S. Williams, J.R. Cantor, R.G. Jones, Immunometabolic interplay in the tumor microenvironment, Cancer Cell 39 (1) (2021) 28–37.
[37] C. Siebel, U. Lendahl, Notch signaling in development, tissue homeostasis, and disease, Physiol. Rev. 97 (4) (2017) 1235–1294.
[38] O. Meurette, P. Mehlen, Notch signaling in the tumor microenvironment, Cancer Cell 34 (4) (2018) 536–548.
[39] B.M. Krishna, S. Jana, J. Singhal, et al., Notch signaling in breast cancer: from pathway analysis to therapy, Cancer letters 461 (2019) 123–131.
[40] J. Qu, Y. Zhou, Y. Li, J. Yu, W. Wang, CASK regulates Notch pathway and functions as a tumor promoter in pancreatic cancer, Arch. Biochem. Biophys. 701 (2021) 108789.
[41] J. Xu, W. Xu, X. Yang, Z. Liu, Y. Zhao, Q. Sun, LncRNA MIR99AHG mediated by FOXA1 modulates NOTCH2/Notch signaling pathway to accelerate pancreatic cancer through sponging miR-3129-5p and recruiting ELAVL1, Cancer Cell Int. 21 (1) (2021) 674.
[42] S. Chen, K. Cai, D. Zheng, et al., RHBDL2 promotes the proliferation, migration, and invasion of pancreatic cancer by stabilizing the N1ICD via the OTUD7B and activating the Notch signaling pathway, Cell Death Dis. 13 (11) (2022) 945.
[43] X. Wang, H. Chen, R. Jiang, et al., Interleukin-17 activates and synergizes with the notch signaling pathway in the progression of pancreatic ductal adenocarcinoma, Cancer letters 508 (2021) 1–12.
[44] L. Wang, L. Sun, J. Huang, M. Jiang, Cyclin-dependent kinase inhibitor 3 (CDKN3) novel cell cycle computational network between human non-malignancy associated hepatitis/cirrhosis and hepatocellular carcinoma (HCC) transformation, Cell Prolif. 44 (3) (2011) 291–299.
[45] M. Malumbres, M. Barbacid, Cell cycle, CDKs and cancer: a changing paradigm, Nat. Rev. Cancer 9 (3) (2009) 153–166.
[46] S.W. Lee, C.L. Reimer, L. Fang, M.L. Iruela-Arispe, S.A. Aaronson, Overexpression of kinase-associated phosphatase (KAP) in breast and prostate cancer and inhibition of the transformed phenotype by antisense KAP expression, Mol. Cell Biol. 20 (5) (2000) 1723–1732.
[47] T. Li, H. Xue, Y. Guo, K. Guo, CDKN3 is an independent prognostic factor and promotes ovarian carcinoma cell proliferation in ovarian cancer, Oncol. Rep. 31 (4) (2014) 1825–1831.
[48] Y. Yu, X. Jiang, B.S. Schoch, R.S. Carroll, P.M. Black, M.D. Johnson, Aberrant splicing of cyclin-dependent kinase-associated protein phosphatase KAP increases proliferation and migration in glioblastoma, Cancer Res. 67 (1) (2007) 130–138.
[49] C. Xing, H. Xie, L. Zhou, et al., Cyclin-dependent kinase inhibitor 3 is overexpressed in hepatocellular carcinoma and promotes tumor cell proliferation, Biochemical and biophysical research communications 420 (1) (2012) 29–35.

[50] J. Ma, W. Zhou, Y. Yuan, B. Wang, X. Meng, PSMD12 interacts with CDKN3 and facilitates pancreatic cancer progression, Cancer Gene Ther. 30 (8) (2023) 1072–1083.
[51] J. Zhang, H. Wang, Y. Wang, W. Dong, Z. Jiang, G. Yang, Substrate-mediated gene transduction of LAMA3 for promoting biological sealing between titanium surface and gingival epithelium, Colloids and surfaces B, Biointerfaces 161 (2018) 314–323.
[52] S.F. Xu, Y. Zheng, L. Zhang, et al., Long non-coding RNA LINC00628 interacts epigenetically with the LAMA3 promoter and contributes to lung adenocarcinoma, Mol. Ther. Nucleic Acids 18 (2019) 166–182.
[53] C. Shu, W. Wang, L. Wu, et al., LINC00936/microRNA-221-3p regulates tumor progression in ovarian cancer by interacting with LAMA3, Recent Pat. Anti-Cancer Drug Discov. 18 (1) (2023) 66–79.
[54] C. Yang, Z. Liu, X. Zeng, et al., Evaluation of the diagnostic ability of laminin gene family for pancreatic ductal adenocarcinoma, Aging 11 (11) (2019) 3679–3703.
[55] L. Buscail, B. Bournet, P. Cordelier, Role of oncogenic KRAS in the diagnosis, prognosis and treatment of pancreatic cancer, Nat. Rev. Gastroenterol. Hepatol. 17 (3) (2020) 153–168.
[56] S.F. Bannoura, M.H. Uddin, M. Nagasaka, et al., Targeting KRAS in pancreatic cancer: new drugs on the horizon, Cancer metastasis reviews 40 (3) (2021) 819–835.
[57] A.S. Dhillon, S. Hagan, O. Rath, W. Kolch, MAP kinase signalling pathways in cancer, Oncogene 26 (22) (2007) 3279–3290.
[58] D.A. Fruman, H. Chiu, B.D. Hopkins, S. Bagrodia, L.C. Cantley, R.T. Abraham, The PI3K pathway in human disease, Cell 170 (4) (2017) 605–635.
[59] L.R. Gentry, T.D. Martin, D.J. Reiner, C.J. Der, Ral small GTPase signaling and oncogenesis: more than just 15minutes of fame, Biochim. Biophys. Acta 1843 (12) (2014) 2976–2988.
[60] R.M. Carr, D. Vorobyev, T. Lasho, et al., RAS mutations drive proliferative chronic myelomonocytic leukemia via a KMT2A-PLK1 axis, Nat. Commun. 12 (1) (2021) 2901.
[61] S. Fujita-Sato, J. Galeas, M. Truitt, et al., Enhanced MET translation and signaling sustains K-Ras-Driven proliferation under anchorage-independent growth conditions, Cancer Res. 75 (14) (2015) 2851–2862.
[62] J. Du, Y. He, W. Wu, et al., Targeting EphA2 with miR-124 mediates Erlotinib resistance in K-RAS mutated pancreatic cancer, J. Pharm. Pharmacol. 71 (2) (2019) 196–205.